Phonon Transport through Point Contacts between Graphitic Nanomaterials

Juekuan Yang,[1,2] Meng Shen,[3] Yang Yang,[2] William J. Evans,[4] Zhiyong Wei,[1] Weiyu Chen,[1] Alfred A. Zinn,[5] Yunfei Chen,[1] Ravi Prasher,[6,7] Terry T. Xu,[8] Pawel Keblinski,[3] and Deyu Li[2,*]

[1]*School of Mechanical Engineering and Jiangsu Key Laboratory for Design and Manufacture of Micro-Nano Biomedical Instruments, Southeast University, Nanjing 210096, People's Republic of China*

[2]*Department of Mechanical Engineering, Vanderbilt University, Nashville, Tennessee 37235, USA*

[3]*Department of Materials Science and Engineering, Rensselaer Polytechnic Institute, Troy, New York 12180, USA*

[4]*Rensselaer Nanotechnology Center, Rensselaer Polytechnic Institute, Troy, New York 12180, USA*

[5]*Advanced Technology Center, Lockheed Martin Space Systems Company, Palo Alto, California 94304, USA*

[6]*Sheetak Incorporated, Austin, Texas 78744, USA*

[7]*School for Engineering of Matter, Transport, and Energy, Arizona State University, Tempe, Arizona 85287, USA*

[8]*Department of Mechanical Engineering and Engineering Science, The University of North Carolina at Charlotte, Charlotte, North Carolina 28223, USA*

(Received 7 June 2013; revised manuscript received 29 January 2014; published 19 May 2014)

Measurements of thermal transport through contacts between individual multiwall carbon nanotubes show that, contrary to common expectation, the normalized contact thermal conductance per unit area depends linearly on the tube diameter. The result is corroborated with and extended to multilayer graphene nanoribbons through molecular dynamics simulations. Semiquantitative analyses show that these intriguing observations are consistent with an explanation based on an unexpectedly large phonon mean free path in the *c*-axis direction of graphite, phonon reflection at free surfaces, and phonon focusing in highly anisotropic graphitic materials.

DOI: 10.1103/PhysRevLett.112.205901 PACS numbers: 65.80.-g, 81.07.Lk

Carbon nanotubes (CNTs) and graphene have attracted enormous attention because of their superior properties and promising applications in energy, microelectronics, and biotechnology [1,2]. In terms of energy transport, while a good understanding has been achieved on the transport phenomena within CNTs [3–5] and graphene membranes [6,7], currently, there is no well-accepted explanation of phonon transport at CNT-CNT or graphene-graphene junctions, which hinders progress in important technology fields.

The interest in phonon transport through CNT contacts was raised in using CNTs to tune the thermal properties of nanocomposites [1,8] and for thermal management of electronic devices [9]. It has been shown that the measured thermal conductivity of CNT-polymer composites is one order of magnitude lower than that predicted based on the classical particle mixing theory, which has been attributed to the contact thermal resistance between CNTs and between the CNT and polymer matrix [8]. However, an anomalously low contact thermal conductance has to be assumed to explain the very limited thermal conductivity enhancement observed. In fact, experiments suggested a very low contact thermal conductance between single-wall CNTs (~3 pW/K) [9,10], more than one order of magnitude lower than the corresponding numerical prediction (~50 pW/K) [10]. To date, for both modeling [10–16] and experimental results [9,10], if the contact thermal conductance is normalized with the contact area, the derived value is much lower than that between two neighboring atomic layers in graphite and no explanation can be found. More recently, graphene has been used to enhance the thermal property of polymer composites with the hope that the larger contact areas between graphene membranes can solve the contact issue [17]; however, the measured enhancement is still much lower than expectation. These observations point to a lack of fundamental understanding of phonon transport at the contacts between graphitic nanomaterials.

Here, we report on systematic measurements of thermal conductance at the point contact between two multiwall CNTs (MWCNTs). The measurements were performed with a microdevice that has been used to measure thermophysical properties of various nanotubes [4,5], nanoribbons [18,19], and nanowires [20,21]. Using a micromanipulator, an individual MWCNT was broken into two segments and transferred to the device, forming a cross contact between the two suspended membranes [Fig. 1(a)]. After measuring the total thermal resistance of this cross-contact sample, one segment was removed and the other was realigned to bridge the two membranes [Fig. 1(b)]. The length of the single MWCNT segment between the two membranes L_S was adjusted to be close to that of the total heat transfer route of the cross-contact sample between the two membranes L_C. From these two measurements, the contact thermal resistance, R_C (or conductance, $G_C = 1/R_C$) between the two MWCNTs can be extracted [22].

Five MWCNT samples of different diameters have been measured (see Table I and Figs. S1–S4 in [22]). Figure 2(a)

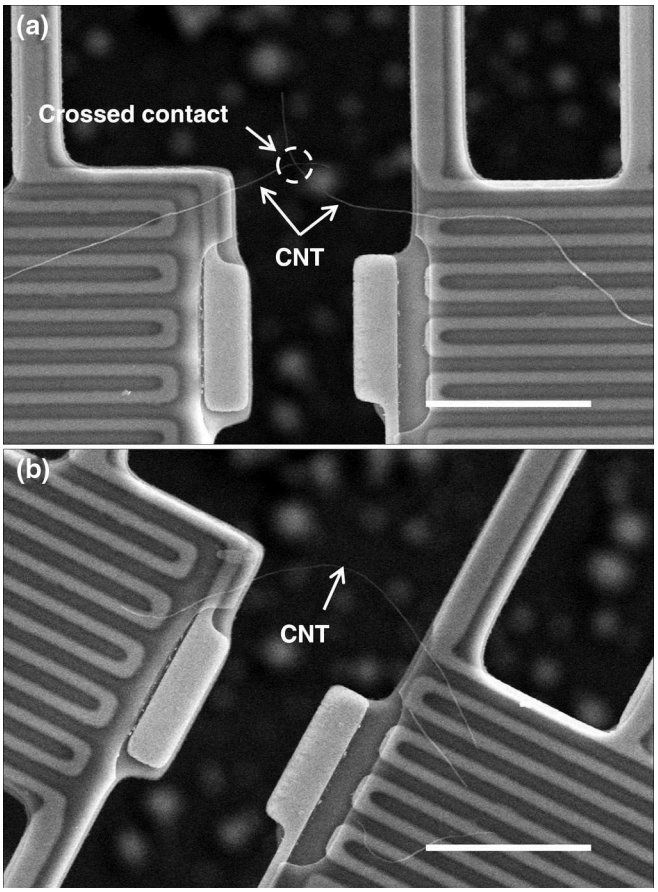

FIG. 1. (a) A scanning electron microscopy (SEM) micrograph of one measured sample composed of two MWCNT segments forming a cross contact between the heat source and sink. Scale bar: 7.5 μm. (b) One of the two segments is realigned on the microdevice to evaluate the thermal resistance of the MWCNT segments in the cross contact sample. Scale bar: 7.5 μm. The diameter of this tube is 63 nm.

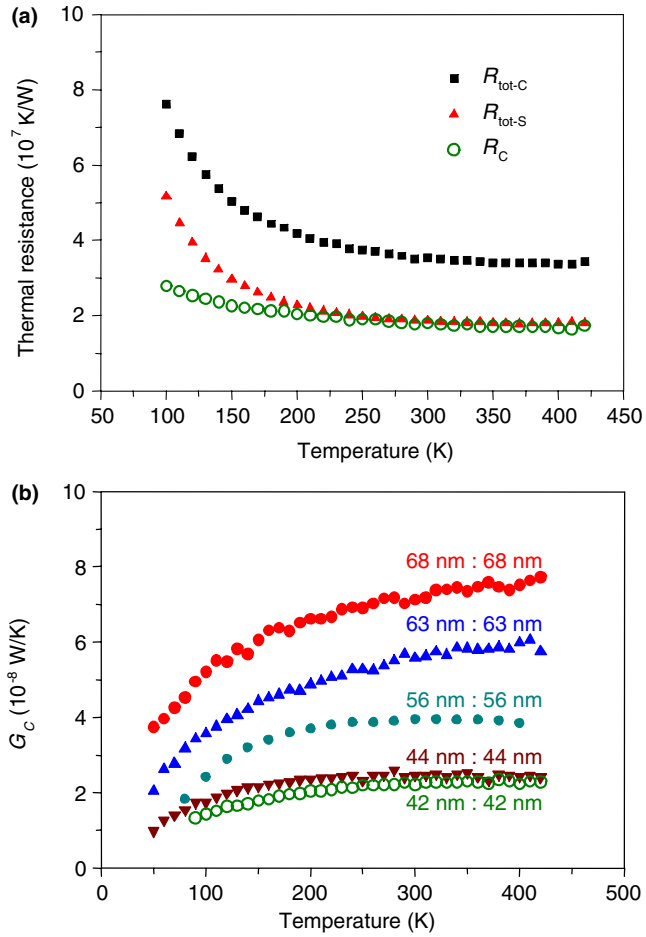

FIG. 2 (color online). (a) The measured thermal resistance for the 63 nm diameter tube. $R_{tot\text{-}C}$, and $R_{tot\text{-}S}$ are measured thermal resistance for the cross-contact sample [Fig. 1(a)] and the single CNT segment [Fig. 1(b)], respectively. R_C is the derived contact thermal resistance. To keep the figure clear, only the data points above 100 K are given. (b) The measured total contact thermal conductance. The labels in (b) denote the diameters of the two segments forming a crossed contact.

shows the measured thermal resistance for the 63 nm diameter tube, which indicates that the resistance of the point contact is approximately equal to that of the MWCNTs for $T > 175$ K. This large R_C is well beyond the measurement uncertainty, which is less than 10% above 150 K for most samples [22]. It is worth noting that the ratio of R_C to the total thermal resistance only varies marginally for all the samples. Figure 2(b) plots the contact thermal conductance, G_C, as a function of temperature, which clearly indicates that G_C increases with the tube diameter. This is very reasonable because the contact area between two CNTs increases for larger tubes.

To further understand the results, we seek to normalize G_C with the contact area (A) between the two CNTs, which is evaluated using the Maugis model [22,23], as given in Table I. We expect that the normalized contact thermal conductance per unit area, G_{CA}, should be approximately the same for different diameter tubes. However, the results [Fig. 3(a)] clearly show that G_{CA} still increases with the tube diameter (D), a trend totally unexpected. Interestingly, if we further normalize G_{CA} with D, within the measurement uncertainty, the five curves of G_{CA}/D overlap with each other, as shown in Fig. 3(b).

TABLE I. Geometry parameters of the five samples measured. L_{CM-C} and L_{CM-S} are the length of the MWCNT on the membrane for the cross-contact sample and the single CNT segment, respectively. α is the tube contact angle.

D (nm)	t (nm)	α (°)	A(nm^2)	L_C (μm)	L_S (μm)	L_{CM-C} (μm)	L_{CM-S} (μm)
68	26	64	57.5	11.7	11.4	>5/>5	>5/4.2
63	24.8	107	48.7	9.3	10.0	>5/>5	>5/>5
56	22	99	39.3	7.9	8.6	>5/>5	2.3/>5
44	14.8	115	31.0	7.4	7.9	>5/>5	2.3/>5
42	14.3	122	31.0	9.1	7.3	>5/>5	1.4/>5

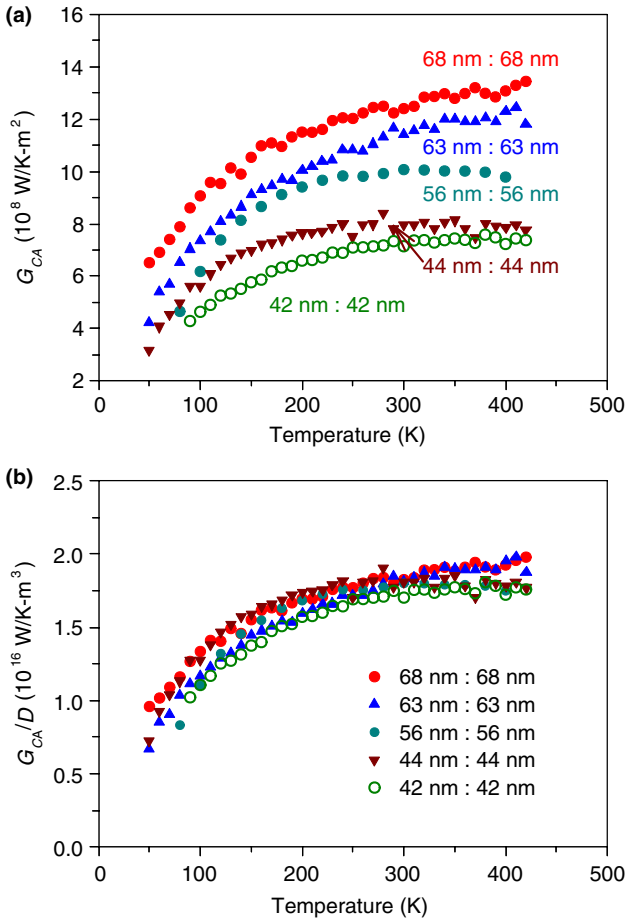

FIG. 3 (color online). (a) The contact thermal conductance per unit area. (b) The contact thermal conductance per unit area normalized with the tube diameter, which approximately collapses into one line. Analyses show that G_C is proportional to $D^{2.4}$ and the contact area is proportional to $D^{1.4}$. The labels in the figure denote the diameters of the two segments forming a crossed contact.

In order to verify the intriguing relation between G_{CA} and the tube diameter, we use molecular dynamics (MD) to study a nanoscale junction between two stacks of multilayer graphene nanoribbons each containing from one to eight atomic graphite layers [22]. The interactions between the top stack and the bottom stack were limited to a small interaction window as depicted in Fig. 4. The width of the ribbons is 2.54 nm, while the length was varied to assess the effect of the finite ribbon length on the contact conductance. Periodic boundary conditions were used for in-plane directions so that the MD system corresponds to two thin films with a slit contact [24]. For this analysis, the underlying mechanism of phonon transport at the nanoscale junction is the same as that between MWCNTs, which will help to disclose the physics of phonon transport between two graphitic nanomaterials. One advantage of modeling graphene nanoribbons is that the contact area between the two ribbons is well-defined and does not change as the ribbon thickness increases.

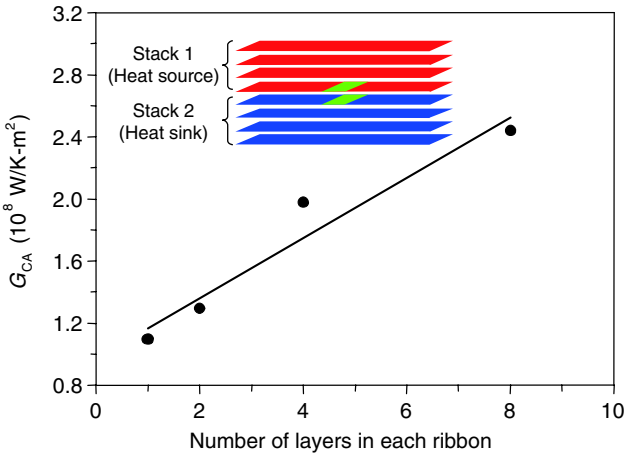

FIG. 4 (color online). MD results showing the linear dependence of the contact thermal conductance per unit area on the number of layers. Inset: a schematic of MD simulation domain.

The MD results [Fig. 4] indicate that G_{CA} increases approximately linearly with the number of layers in each ribbon, which confirms the observed linear dependence of G_{CA} on the MWCNT diameter. It is worth noting that transmission electron microscopy studies have confirmed that the wall thickness (t) of the MWCNTs increases with the tube diameter (see Table I). Therefore, both the MD results and the experimental data indicate that G_{CA} increases with the number of layers in each tube or ribbon.

These results disclose a different view from the classical picture of point contact thermal resistance. The point contact thermal resistance is classically treated as a combination of diffusive resistance and ballistic resistance (or Sharvin resistance), and the relative importance of these two mechanisms depends on the ratio of the characteristic size of the point contact and the phonon mean free path (mfp) [25]. For diffusive resistance, G_{CA} decreases with the contact area, which is exactly opposite to our observation. The Sharvin resistance for unit area does not change with the contact size, which is also different from our observations. The results cannot be explained using the well-established models for thermal boundary resistance, such as the acoustic or diffuse mismatch model, either [26]. In both models, interfacial thermal conductance per unit area is determined by the materials in contact and the morphology of the interface, but not related to the size of the samples in contact, as shown in our results.

It is worth noting that these classical models are established by considering phonon transport through a contact or interface between two bulk isotropic materials. Our results, however, are the first experimental measurement of thermal resistance of a nanoscale contact between two free standing anisotropic nanostructures. We attribute the unexpected diameter dependence of G_{CA} to phonon reflection at free surfaces and an unexpectedly large intrinsic phonon mfp in the c axis of graphite (l_c), and

argue that the highly anisotropic nature of graphitic materials also plays an important role.

Traditionally, it is widely believed that l_c for graphite is only a few nm [27,28]. However, this very short mfp is obtained by assuming that all phonon modes in graphite contribute to thermal transport in the c-axis direction, which is problematic because van der Waals (vdW) interactions between different atomic layers in graphite cannot sustain transport of the high frequency phonons existing in each atomic layer. If we consider this effect, phenomenological modeling indicates that l_c could be well over a hundred nanometers [22], which has also been confirmed by our recent MD simulation with graphite thin films [29]. It is worth noting that very recently, more detailed calculations based on a full phonon dispersion indicated that l_c could attain a value of 20 nm [30], much longer than just a few nanometers. Furthermore, if l_c for graphite is only a few nm, which is less than the wall thickness of the CNT we measured, the contact thermal resistance between two CNTs should be simply Sharvin-type resistance and G_{CA} should be independent of the wall thickness of the CNTs.

If l_c is over 100 nm, there are chances for phonons to travel ballistically through the nanoscale contact and be reflected back into the emitting side, which effectively reduces the thermal conductance of the contact. To illustrate this effect on the dependence of G_{CA} on the thickness of the tube or ribbon, we performed simplified Monte Carlo (MC) simulations with a ray-tracing method using a two-dimensional model, as shown in Fig. 5. Two slabs of 200 nm length and 10–30 nm thick serve as a heat source and a heat sink, respectively, and make a junction of 6 nm width, through which phonons can transmit. l_c is assumed to be 100 nm, and 5×10^5 phonons per nm in height were initialized in the heat source with random position and random direction. After equilibrium, we count the number of phonons scattered in the heat sink, which after normalized with the difference in the phonon number densities of the heat source and the heat sink, represents the contact conductance [22]. The simulation results indicate that since the free surfaces are very close to the slit, a significant portion of phonons transmitted through the slit could be reflected back into the heat source, and this portion increases as the slabs get thinner, which means that the conductance reduces for thinner slabs, consistent with our experimental results and MD simulations.

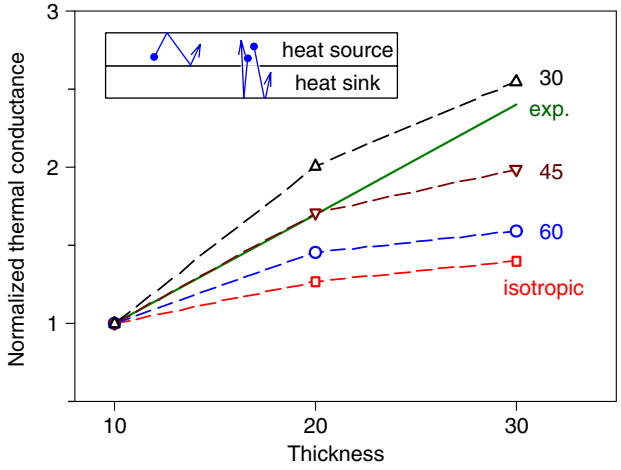

FIG. 5 (color online). The normalized thermal conductance with respect to the 10 nm thick case. The number labels denote the allowable angles for phonon transport directions from the c axis direction. The best linear fit of the experiment data (G_{CA}) at room temperature given in Fig. 3 is also presented.

The obtained normalized thermal conductance with respect to the 10 nm thick case is shown in Fig. 5. For isotropic phonon transport, the thermal conductance does increase with the slab thickness; however, the escalation rate is much lower than our experimental observation. This discrepancy can be attributed to the well-recognized phonon focusing effect in highly anisotropic materials [31,32]. In graphite, the phonon group velocities are focused to be along both the in-plane and cross-plane directions, as can be seen from the iso-energy surfaces in a recent publication [32]. Therefore, phonons responsible for cross-plane thermal transport do not propagate along large angles from the c axis. To reflect this fact, we can restrict the angle of phonon propagation in our MC simulation. As shown in Fig. 5, if we limit the possible angles for phonon transport from the c-axis direction, the enhancement of G_{CA} with the slab thickness becomes more and more pronounced as the allowable phonon propagation angle from the c-axis direction reduces.

We point out that for both experimental and MD studies, the obtained G_{CA} is still far below the upper bound that can be obtained from theoretical reasoning. The upper bound for the conductance in the limit of very large number of layers can be simply regarded as the interlayer thermal conductance between two neighboring atomic layers in bulk graphite. Assuming the interfaces can be treated as resistors connected in series, the interlayer conductance can be estimated as $G_{\mathrm{CA,upper}} = k/a$, where k is the cross-plane graphite thermal conductivity and a is the spacing between planes. With $k = 6.8\ \mathrm{W/m\,K}$ [33] and $a = 0.34$ nm, $G_{\mathrm{CA,upper}} = 20\ \mathrm{GW/m^2\,K}$, which is still one order of magnitude higher than the experimental data, reflecting that the wall thickness of the MWCNTs is still much less than l_c.

It is worth noting that three mechanisms coupled together leading to the observed intriguing contact thermal conductance. Inspired by the observation here, we have demonstrated a c-axis phonon mfp of $\sim$145 nm through MD simulation of graphite thin films [29]. The effects of phonon reflection at free surfaces are physically straightforward and have been further verified by a separate theoretical analysis with a thin film on a substrate [34]. Phonon focusing in graphite is well recognized, and even though most attention has been paid to the effects of phonon focusing into the in-plane directions, the same

mechanism will also lead to phonon focusing into the *c*-axis direction, as can be easily seen from the iso-energy surfaces in Ref. [32]. The obtained diameter or thickness dependent contact thermal conductance should provide new insights into tuning thermal properties of CNT or graphene-based nanocomposites.

We thank the financial support from the U.S. National Science foundation (Grants No. 0821604, No. 1067213, and No. 1308550), from Lockheed Martin Corporate, from the National Natural Science Foundation of China (Grant No. 51176032), from the National Basic Research Program of China (Grant No. 2011CB707605), from the Office of Naval Research (Grant No. N00014-07-1-0723), and from Research Project of State Key Laboratory of Mechanical System and Vibration MSV201413. A portion of this research was performed at Oak Ridge National Laboratory's Center for Nanophase Materials Sciences and Cornell NanoScale Facility, a member of the National Nanotechnology Infrastructure Network, which is supported by the National Science Foundation (Grant No. ECS-0335765). The authors thank Dr. Yann Chalopin, Dr. Natalio Mingo, Dr. Vikas Varshney, Dr. Ajit Roy, Dr. Yuping He, Dr. Giulia Galli, and Dr. Alan McGaughey for valuable discussions and Dr. Timothy Gutu for his help in TEM studies.

*deyu.li@vanderbilt.edu

[1] R. H. Baughman, A. A. Zakhidov, and W. A. de Heer, Science **297**, 787 (2002).
[2] A. K. Geim, Science **324**, 1530 (2009).
[3] J. Hone, M. Whitney, C. Piskoti, and A. Zettl, Phys. Rev. B **59**, R2514 (1999).
[4] P. Kim, L. Shi, A. Majumdar, and P. L. McEuen, Phys. Rev. Lett. **87**, 215502 (2001).
[5] C. Yu, L. Shi, Z. Yao, D. Li, and A. Majumdar, Nano Lett. **5**, 1842 (2005).
[6] A. A. Balandin, S. Ghosh, W. Bao, I. Calizo, D. Teweldebrhan, F. Miao, and C. N. Lau, Nano Lett. **8**, 902 (2008).
[7] J. H. Seol *et al.*, Science **328**, 213 (2010).
[8] F. H. Gojny, M. H. G. Wichmann, B. Fiedler, I. A. Kinloch, W. Bauhofer, A. H. Windle, and K. Schulte, Polymer **47**, 2036 (2006).
[9] D. Estrada and E. Pop, Appl. Phys. Lett. **98**, 073102 (2011).
[10] R. S. Prasher, X. J. Hu, Y. Chalopin, N. Mingo, K. Lofgreen, S. Volz, F. Cleri, and P. Keblinski, Phys. Rev. Lett. **102**, 105901 (2009).
[11] Y. Chalopin, S. Volz, and N. Mingo, J. Appl. Phys. **105**, 084301 (2009).
[12] H. Zhong and J. R. Lukes, Phys. Rev. B **74**, 125403 (2006).
[13] Z. Xu and M. J. Buehler, ACS Nano **3**, 2767 (2009).
[14] P. A. Greaney and J. C. Grossman, Phys. Rev. Lett. **98**, 125503 (2007).
[15] V. Varshney, S. S. Patnaik, A. K. Roy, and B. L. Farmer, J. Phys. Chem. C **114**, 16223 (2010).
[16] S. Kumar and J. Y. Murthy, J. Appl. Phys. **106**, 084302 (2009).
[17] T. Kuilla, S. Bhadra, D. Yao, N. H. Kim, S. Bose, and J. H. Lee, Prog. Polym. Sci. **35**, 1350 (2010).
[18] L. Shi, Q. Hao, C. Yu, N. Mingo, X. Kong, and Z. L. Wang, Appl. Phys. Lett. **84**, 2638 (2004).
[19] J. Yang *et al.*, Nat. Nanotechnol. **7**, 91 (2012).
[20] D. Li, Y. Wu, P. Kim, L. Shi, P. Yang, and A. Majumdar, Appl. Phys. Lett. **83**, 2934 (2003).
[21] A. I. Hochbaum, R. Chen, R. D. Delgado, W. Liang, E. C. Garnett, M. Najarian, A. Majumdar, and P. Yang, Nature (London) **451**, 163 (2008).
[22] See Supplemental Material at http://link.aps.org/supplemental/10.1103/PhysRevLett.112.205901 for further details.
[23] D. Maugis, J. Colloid Interface Sci. **150**, 243 (1992).
[24] V. Varshney (private communication) Separate MD simulations by V. Varshney *et al.* obtained similar trend with two graphene nanoribbons forming a cross contact without periodic boundary conditions.
[25] R. Prasher, Nano Lett. **5**, 2155 (2005).
[26] E. T. Swartz and R. O. Pohl, Rev. Mod. Phys. **61**, 605 (1989).
[27] M. Shen, P. K. Schelling, and P. Keblinski, Phys. Rev. B **88**, 045444 (2013).
[28] T. Tanaka and H. Suzuki, Carbon **10**, 253 (1972).
[29] Z. Wei, J. Yang, W. Chen, K. Bi, D. Li, and Y. Chen, Appl. Phys. Lett. **104**, 081903 (2014).
[30] M. M. Sadeghi, I. Jo, and L. Shi, Proc. Natl. Acad. Sci. U.S.A. **110**, 16321 (2013).
[31] J. P. Wolfe, *Imaging Phonons* (Cambridge University Press, Cambridge, England, 1998).
[32] Z. Wei, Y. Chen, and C. Dames, Appl. Phys. Lett. **102**, 011901 (2013).
[33] R. Taylor, Philos. Mag. **13**, 157 (1966).
[34] Z. Liang and P. Keblinski (to be published).